



# **Fluorescence Correlation Spectroscopy**

## An Introduction to its Concepts and Applications

**Petra Schwille and Elke Haustein**  
Experimental Biophysics Group  
Max-Planck-Institute for Biophysical Chemistry  
Am Fassberg 11  
D-37077 Göttingen  
Germany

# Table of Contents

<b>TABLE OF CONTENTS</b>	<b>1</b>
<b>1. INTRODUCTION</b>	<b>3</b>
<b>2. EXPERIMENTAL REALIZATION</b>	<b>5</b>
2.1. ONE-PHOTON EXCITATION	5
2.2. TWO-PHOTON EXCITATION	7
2.3. FLUORESCENT DYES	9
<b>3. THEORETICAL CONCEPTS</b>	<b>10</b>
3.1. AUTOCORRELATION ANALYSIS	10
3.2. CROSS-CORRELATION ANALYSIS	18
<b>4. FCS APPLICATIONS</b>	<b>21</b>
4.1. CONCENTRATION AND AGGREGATION MEASUREMENTS	21
4.2. CONSIDERATION OF RESIDENCE TIMES: DETERMINING MOBILITY AND MOLECULAR INTERACTIONS	23
4.2.1 DIFFUSION ANALYSIS	23
4.2.2 CONFINED AND ANOMALOUS DIFFUSION	24
4.2.3 ACTIVE TRANSPORT PHENOMENA IN TUBULAR STRUCTURES	24
4.2.4 DETERMINATION OF MOLECULAR INTERACTIONS	26
4.2.5 CONFORMATIONAL CHANGES	27
4.3. CONSIDERATION OF CROSS-CORRELATION AMPLITUDES: A DIRECT WAY TO MONITOR ASSOCIATION/DISSOCIATION AND ENZYME KINETICS	28
4.4. CONSIDERATION OF FAST FLICKERING: INTRAMOLECULAR DYNAMICS AND PROBING OF THE MICROENVIRONMENT	30
<b>5. CONCLUSIONS AND OUTLOOK</b>	<b>31</b>
<b>6. REFERENCES</b>	<b>32</b>

# 1. Introduction

Currently, it is almost impossible to open your daily newspaper without stumbling over words like *gene manipulation*, *genetic engineering*, *cloning*, etc. that reflect the tremendous impact of life sciences to our modern world. Press coverage of these features has long left behind the stage of merely reporting scientific facts. Instead, it focuses on general pros and cons, and expresses worries about what scientists have to do and what to refrain from. However, many of these discussions and speculations suffer from a certain vagueness as they tend to disregard that living systems are extremely complicated. Many biological mechanisms are barely known to exist, let alone fully understood. Therefore, major goals of current biological research are not only the identification, but also the precise physico-chemical characterization of elementary processes on the level of individual proteins and nucleic acids. These molecules are believed to be the smallest functional units in biological systems.

To address these minute quantities, very sensitive techniques are required. Among those that allow even single molecule measurements are *atomic force microscopy* (AFM) or *fluorescence spectroscopy*. One outstanding feature of the latter is its comparable noninvasiveness, which makes it perfectly suited for measurements inside living cells.

*Fluorescence correlation spectroscopy* (FCS) is one of the many different modes of high-resolution spatial and temporal analysis of extremely low concentrated biomolecules. In contrast to other fluorescence techniques, the parameter of primary interest is not the emission intensity itself, but rather spontaneous intensity fluctuations caused by the minute deviations of the small system from thermal equilibrium. In general, all physical parameters that give rise to fluctuations in the fluorescence signal are accessible by FCS. It is, for example, rather straightforward to determine local concentrations, mobility coefficients or characteristic rate constants of inter- or intramolecular reactions of fluorescently labeled biomolecules in nanomolar concentrations.

Fluorescence correlation spectroscopy has been developed in the early seventies as a special case of relaxation analysis. Classical relaxation methods induce certain kinds of external perturbations such as temperature or pressure jumps to a reaction system, and gain information about involved kinetic parameters from the way the system returns back to equilibrium. The novel concept of FCS with respect to these classical techniques is to take advantage of the minute spontaneous fluctuations of physical parameters that are somehow reflected by the fluorescence emission of the molecules. Such fluctuations are incessantly occurring at ambient temperatures and are generally represented as (unwanted) noise patterns of the measured signal, in our case fluorescence. The fluctuations can be quantified in their strength and duration by temporally autocorrelating the recorded intensity signal, a mathematical procedure that gave the technique its name. Autocorrelation analysis provides a measure for the self-similarity of a time series signal and therefore describes the persistence of information carried by it. Essential information about processes governing molecular dynamics can thus be derived from the temporal pattern by which fluorescence fluctuations arise and decay.

At its first introduction by Madge, Elson and Webb in 1972, FCS was applied to measure diffusion and chemical dynamics of DNA-drug intercalation. This pioneering study was then followed by a number of other publications by many different groups describing, e.g., attempts to determine particle concentration, translational and rotational mobility in two or three dimensions,

even in the cellular environment or in flow systems. Nevertheless, these early measurements suffered from poor signal-to-noise ratios, mainly because of low detection efficiency, large ensemble numbers and insufficient background suppression.

Imagine trying to find out if a friend had entered or left an overcrowded shopping center without a call to the information desk. Unless you are holding hands, this is next to impossible. And now imagine watching your friend in your living room. In the latter case you simply can't fail to notice him (or her) coming or leaving. This is the basic concept of FCS: Make the number of observed molecules low enough so that each of them contributes substantially to the measured signal. Then and only then, one can truly perform analyses of spontaneous, non-coordinated fluctuations.

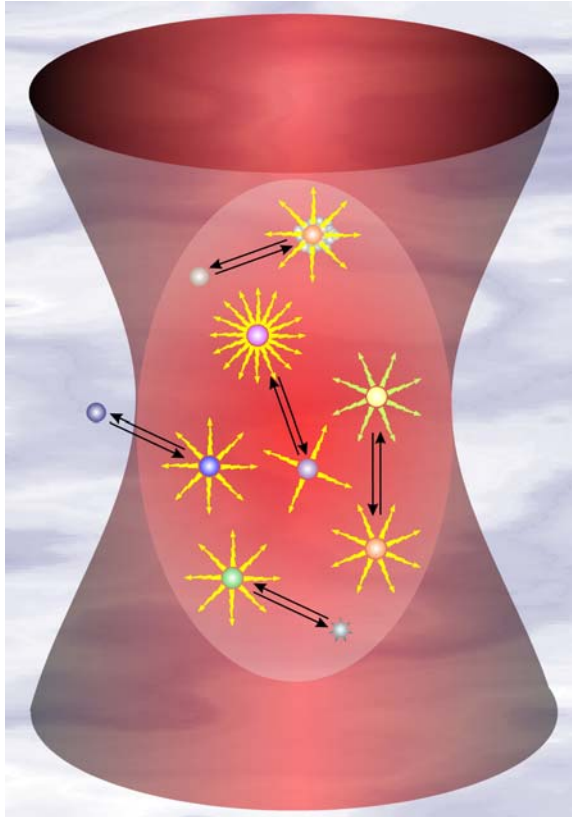


**Figure 1: Molecular mechanisms that might give rise to fluorescence fluctuations comprise particle movements, conformational changes, chemical or photophysical reactions.**

volume of an *E.coli* bacterial cell, concentrations in the nanomolar range are optimal for FCS measurements. Under these circumstances, the signal fluctuations induced by molecules diffusing into or out of the focal volume are large enough to yield good signal-to-noise ratios. During the time a particle spends in the focus, chemical or photophysical reactions or conformational changes may alter the emission characteristics of the fluorophore and give rise to additional fluctuations in the detected signal.

The principle of FCS can no longer be called a recent invention. It is a versatile method that already has demonstrated its vast possibilities for many different problems. Nowadays, it is -

It is obvious that FCS can only function properly if one somehow manages to reduce the concentrations and observation volumes such that only few molecules are simultaneously detected, and at the same time increase the fluorescence photon yield per single molecule. A major improvement could be made by using efficient fluorescent dyes to label the molecules of interest, strong and stable light sources like lasers, and ultrasensitive detectors, e.g. avalanche photodiodes with single-photon sensitivity. The final breakthrough was achieved in Stockholm by Rigler and his coworkers by combining the FCS technique with confocal detection. Here, the incoming laser light is strongly focused by a high numerical aperture objective (ideally  $NA > 0.9$ ) to a diffraction limited spot. Only the few fluorophores within the illuminated region are excited. In order to limit the detection volume also in axial direction, a pinhole is introduced in the image plane, which blocks all light not coming from the focal region.

To date, most FCS measurements are performed on fluorescently labeled biomolecules diffusing in aqueous buffer solution. Because of the most elegant way of limiting the detection volume to less than one femtoliter, i.e. approximately the

together with other confocal fluorescence readout techniques - one of the standard tools used for high-throughput screening, combining very short data acquisition times with straightforward analysis.

Only recently, an increasing number of intracellular measurements has been reported. The mobility of proteins and DNA- or RNA-fragments within the cytosol or other cell organelles belong to the most prominent measurement parameters. An increasing number of studies is now devoted to the analysis of molecular (e.g. protein-protein) interactions or translocation processes. One reason this has not been done earlier is certainly the poor signal quality due to autofluorescence and light absorption or scattering. Another problem consists in the limited supply of dye molecules within the cell, which may lead to irreversible photobleaching.

## 2. Experimental Realization

### 2.1. One-Photon Excitation

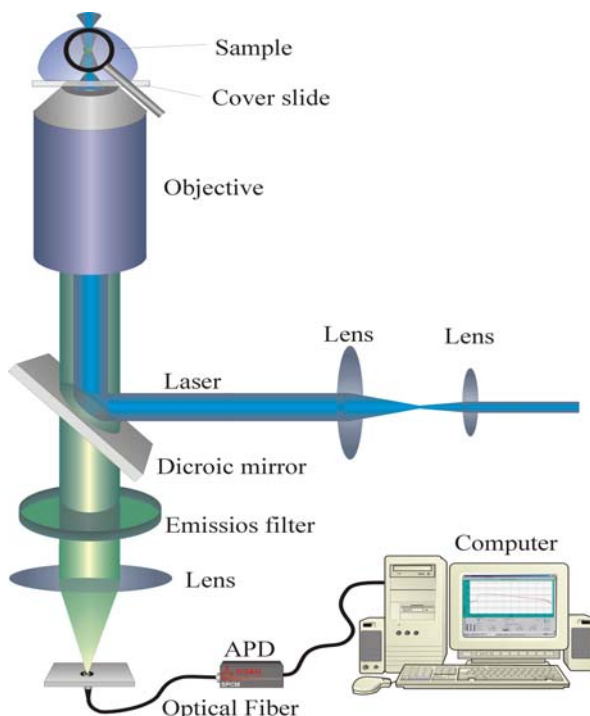


**Figure 2:** Schematic drawing of an FCS setup

The confocal FCS setup, which has already been mentioned briefly above, is illustrated schematically in figure 2. The exciting radiation provided by a laser beam is directed into a microscope objective via a dichroic mirror and focused on the sample. As the sample molecules are usually dissolved in aqueous solution, water immersion objectives with a high numerical aperture (ideally  $> 0.9$ ) are used. The fluorescence light from the sample is collected by the same objective and passed through the dichroic and the emission filter. The pinhole in the image plane (field aperture) blocks any fluorescence light not originating from the focal region, thus providing axial resolution. Afterwards, the light is focused onto the detector, preferably an avalanche photodiode or a photomultiplier with single photon sensitivity.

Depending on your dye system, you may use Argon- or Argon-Krypton-Lasers, which allow the choice between multiple laser lines and thus

provide a versatile system. Inexpensive alternatives are single-line He-Ne-Lasers or even laser diodes. Depending on the beam quality and diameter of the laser, one might consider inserting a beam expander or an optical filter before the laser beam is coupled into the microscope. The larger the beam diameter, the smaller the resulting focal volume will be. By overfilling the back aperture of your objective, you even get a diffraction limited spot of approximately  $0.5 \mu\text{m}$  in diameter.

The sample carrier depends on your application. For test measurements, a simple cover slide on which you place a drop of the solution will be sufficient. More elaborate measurements can be done in special (sealed) chambers or deep-well slides.

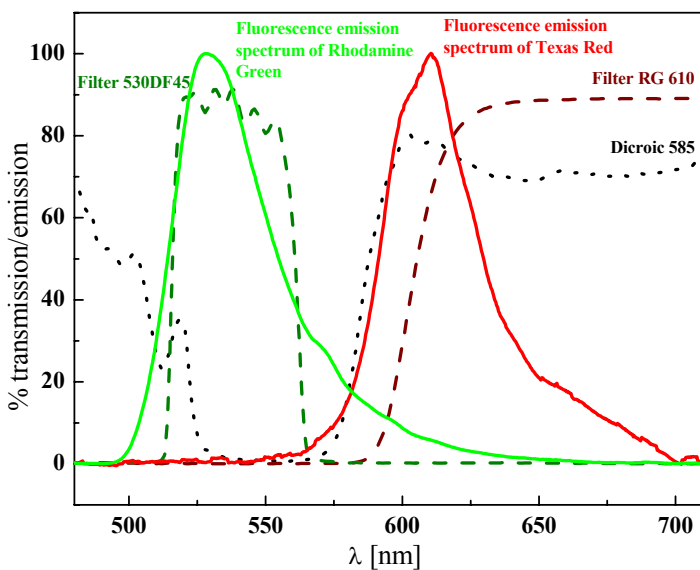


**Figure 3: Fluorescence emission spectra of two dyes and the appropriate filter system for a cross-correlation setup (Courtesy of Katrin Heinze)**

light (Rayleigh scattering) and Raman scattering, which in water is red-shifted  $3380\text{ cm}^{-1}$  relative to the laser line.

The fluorescence signal is usually autocorrelated by a hardware correlator PC card for 10s – 120s. Both the fluorescence signal and the calculated curve are displayed simultaneously on the monitor to facilitate adjustment and control of the setup. Data is saved in ASCII format and can be imported in any math program for further analysis. Fitting routines using the Levenberg-Marquardt non-linear least-square routine have proved very efficient.

When studying for example enzyme-substrate reactions, the change in mass between the substrate and the enzyme-substrate complex is usually much less than one order of magnitude, such that the observed diffusion times differ by less than a factor of two (assuming globular particles). Considering the logarithmic time scale, this makes quantitative analysis rather difficult. A solution to the problem consists in labeling both partners with different colors and only looking at those clinging together. For this purpose, excitation is performed by two different lasers, and the fluorescence light is divided into two channels, simultaneously measuring red and green signal and cross-correlating them to get a direct measure of the reaction efficiency. Introducing an additional dichroic in the emission pathway between the first dichroic and the pinholes splits the fluorescence signal.

The signal-to-noise ratio of the FCS curves depends critically on the filter system. First, there is the dichroic mirror, which serves basically as a wavelength-dependent beam-splitter. It deflects excitation light and transmits the red-shifted fluorescence, but the blocking efficiency for the laser is usually very poor, less than OD3 (three orders of magnitude). Therefore, one or more additional emission filters are required. Bandpass filters adapted to the emission properties of the observed dye are recommended to guarantee high enough detection specificity at sufficient photon yields. Bandwidths of 30-50 nm allow suppression of both scattered laser

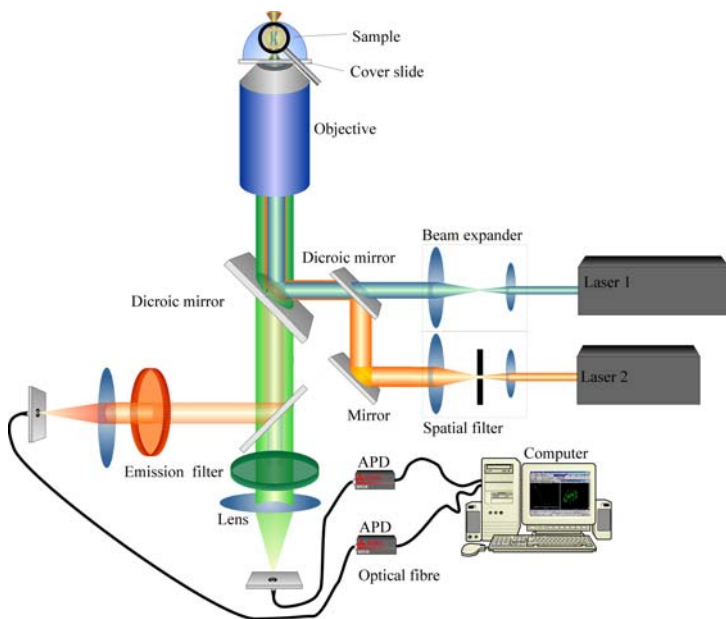


**Figure 4: Dual –color cross-correlation setup**

One of the solutions to this problem is the use of a multi-line laser as suggested by Winkler et al. [Winkler 1999]. Among the severe drawbacks of this technique, however, is the need for perfectly corrected microscope objectives. Moreover, to achieve focal spots of the same size, selective filters that reduce the diameter of the green beam have to be employed. Only recently, another elegant solution has been established. Using two-photon excitation, it is possible to excite two carefully selected spectrally different dyes with only one IR laser line. This technique will be discussed below in more detail.

## 2.2. Two-Photon Excitation

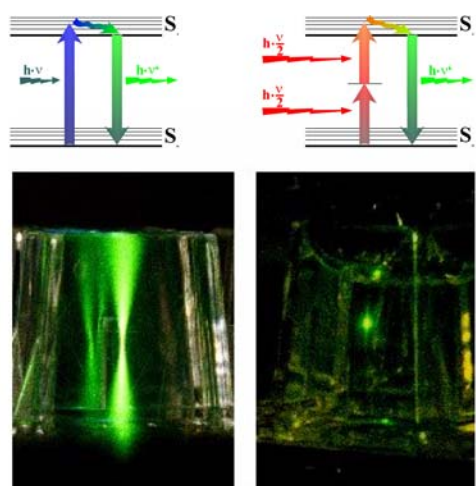


**Figure 5: Comparison between one- and two-photon absorption processes and photographs taken of the excited region**

Now, two emission filters are required, whose transmission spectra ideally should not overlap to minimize crosstalk. As a rule of thumb, the transmission maxima of the bandpass filters should be at least 100 nm apart, if possible.

The experimental realization of a dual-color cross-correlation setup is very demanding, because it also requires exact spatial superposition of the two laser beams, so that the focal volumes overlap. Checking and optimizing the alignment either directly by measuring the illumination profiles with a specifically designed focus scanner or indirectly by FCS calibration measurements can be quite tedious.

Two-photon excitation requires the absorption of two photons of theoretically double the wavelength usually required for the excitation, within the tiny time interval of about one femtosecond ( $10^{-15}$  s). In order to get a reasonable probability of such three-particle events, the photon flux must be extremely high. This means, that not only a high output power is required, but usually also pulsed excitation is used, to get an even higher photon density per pulse relative to the average output power. The joint probability of absorbing two photons per excitation process is proportional to the mean square of the intensity. This results in inherent depth discrimination such that only the immediate vicinity of the objective's focal spot receives sufficient intensity for significant fluorescence excitation.

Intracellular measurements primarily benefit from this

inherent axial resolution, because under two-photon excitation, bleaching really occurs only in the focal region [Denk 1990]. In contrast to this, under one-photon excitation, all fluorophores residing in the double cone above and below the focal spot are excited and bleached, the depth discrimination by the pinhole is quasi an artificial effect, restricted to the detection signal. As cells and tissue also tend to be more tolerant to near infrared radiation and there is less autofluorescence and scattering, multi-photon excitation is becoming more and more popular for biological applications, in particular for confocal scanning microscopy.

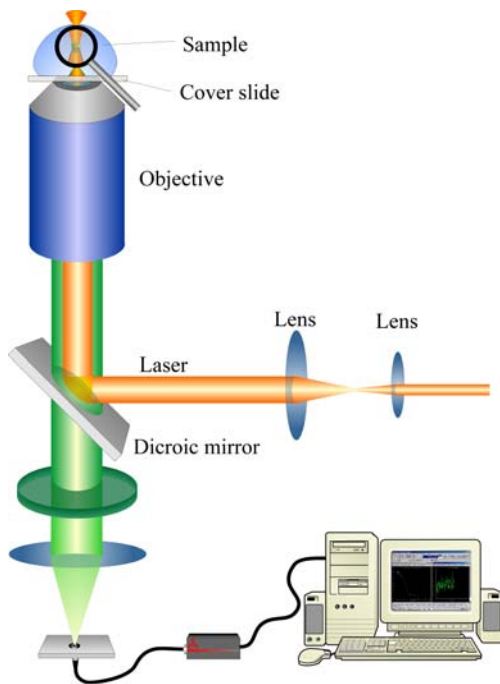


**Figure 6: Two-photon setup**

Unfortunately, determining the two-photon excitation spectra of different dyes turns out quite difficult. As two-photon excitation is a quantum mechanically forbidden process, the selection rules differ greatly from those valid for one-photon processes. The idea of simply taking photons with half the energy required for the transition to the excited state often gives very unsatisfactory results. The experimentally determined two-photon excitation spectrum very often exhibits a significant blue shift relative to the one-photon spectrum, indicating a first transition to a higher excited state. After internal relaxation, the system finally returns to the same excited state as for the one-photon process, and the emission spectra are the same. Maybe because of this complicated, symmetry forbidden absorption process in addition to the pulsed excitation, the maximum number of photons that a dye molecule emits before undergoing photodestruction is significantly lower than for the quantum mechanically allowed processes. Moreover, due to the quadratic intensity dependence, the range of applicable powers is much narrower.

As mentioned above, this dye-specific blue-shift can be used to simultaneously excite two dyes with different emission characteristics to perform two-photon dual color cross-correlation experiments. Only one laser line is required for excitation, and the inherent axial resolution renders pinholes redundant, so that adjustment is greatly simplified. You need, however, to alter the emission filter system with respect to one-photon applications. Shortpass dichroic mirrors and interference filters are required to efficiently block the Rayleigh scattering induced by the excitation laser.

In spite of the experimental difficulties listed above, two-photon excitation combines good signal-to-noise ratio with low invasiveness, especially for sensitive biological applications. The attractiveness is hitherto mainly limited by the lack of commercially available systems and the rather expensive pulsed laser system required.

## 2.3. Fluorescent Dyes

Among the first dyes tested for their suitability in FCS measurements were fluorophores already known from fluorescence spectroscopy and microscopy (e.g. fluorescein), and laser dyes. However, the requirements imposed on a fluorophore in single molecule techniques are not only a high quantum efficiency and large absorption cross section, as in traditional spectroscopy. The most crucial property is the photostability, which must be high enough to enable the dye to withstand the enormous power in the laser focus, which may be of the order of several 100 kW/cm<sup>2</sup>. Fluorescein, in standard applications being considered a rather good fluorophore, photobleaches already at comparably low excitation powers, giving rise to unwanted artifacts in FCS and related methods.



**Figure 7: Colors of different Alexa-Dyes (Molecular Probes).** From left to right: Alexa350, Alexa430, Alexa488, Alexa532, Alexa546, Alexa568, Alexa633, Alexa700, Alexa750. White light is absorbed and generates fluorescence (in the cuvettes). The transmitted light can be seen on the back.

For single molecule applications, it is thus now mostly substituted by the specifically engineered dye Alexa488 (Molecular Probes) with similar absorption and emission characteristics and enhanced photostability. The Alexa dye family exhibits a very large selection of different colors. The absorption maxima range from 350 nm to 750 nm, covering more than the visible spectrum (cf. figure 7). Other suitable dyes are rhodamines such as Rhodamine Green, TMR, Rhodamine B and 6G, and cyanines (Cy2, Cy3, Cy5). It is also important to note that one- and two-photon

properties of dyes can be extremely different. Whereas Cy5 is the red partner in most one-photon cross-correlation and FRET-experiments, it is completely unsuitable for two-photon excitation and must be replaced by Alexa633, for example.

The major common disadvantage of all of these synthetic dyes consists in the fact that you have to specifically label a biological system before performing any experiments. This is often difficult and tedious, especially when you want to do intracellular measurements and need to get the protein of interest back into the cell after labeling. Today, there are also two kinds of autofluorescent proteins, *green fluorescent protein* (GFP) and DsRed. Originally, GFP is produced by the jellyfish *Aequorea Victoria* and the more recently discovered DsRed by the coral *Dictyosoma*, but both proteins and their mutants can be expressed in genetically manipulated cells. Thus, by proper cloning it is possible to “convince” cells to produce the proteins you want already with the fluorescent marker attached to them. Fluorescence microscopy and FCS can then readily be performed without further treatment such as microinjection.

## 3. Theoretical Concepts

### 3.1. Autocorrelation Analysis

Autocorrelation analysis is performed, if you want to focus on one particular species of fluorescent particles. Fluctuations in the fluorescence signal are quantified by temporally autocorrelating the recorded intensity signal. In principle, this autocorrelation routine provides a measure for the self-similarity of a time signal and highlights characteristic time constants of underlying processes.

The number of molecules contained within the focal volume at any time is governed by Poissonian distribution. Therefore, the root mean square fluctuation of the particle number  $N$  is given by

$$\frac{\sqrt{\langle (\delta N)^2 \rangle}}{\langle N \rangle} = \frac{\sqrt{\langle (N - \langle N \rangle)^2 \rangle}}{\langle N \rangle} = \frac{1}{\sqrt{\langle N \rangle}}$$
Equation 1

Since the relative fluctuations become smaller with increasing numbers of measured particles, it is important to minimize the number of molecules in the focal volume. However, the fluorescence signal must still be higher than the residual background signal. If there are too few molecules in the solution, there may be times with no molecule at all in the focus. Roughly, the temporal average of the particle number should be between 0.1 and 1000. The focal volume being about one femtoliter, this corresponds to concentrations between sub-nanomolar ( $< 10^{-9}$  M) and micromolar ( $10^{-6}$  M).

The fluorescence emitted by the molecules in the focal spot is recorded photon by photon. Assuming constant excitation power, the fluctuations of the fluorescence signal are defined as the deviations from the temporal average of the signal:

$$\begin{aligned} \delta F(t) &= F(t) - \langle F(t) \rangle \\ \langle F(t) \rangle &= \frac{1}{T} \int_0^T F(t) dt \end{aligned}$$
Equation 2

If all fluctuations arise only from changes in the local concentration  $\delta C$  within the effective volume  $V_{\text{eff}}$  of the focal spot, the variations may be written as

$$\delta F(t) = \kappa \int_V I_{\text{ex}}(\underline{r}) \cdot S(\underline{r}) \cdot \delta(\sigma \cdot q \cdot C(\underline{r}, t)) \cdot dV$$
Equation 3

The individual parameters listed above are mainly describing the probability of exciting a fluorophore within the focal volume and detecting the emitted photon afterwards due to the final detection efficiency of the setup:

$\kappa$ :	overall detection efficiency
$I_{\text{ex}}(\underline{r})$ :	spatial distribution of the excitation energy with the maximum

$S(\underline{r})$ :	amplitude $I_0$ optical transfer function of the objective-pinhole combination. This determines the spatial collection efficiency of the setup and is dimensionless
$\delta(\sigma \cdot q \cdot C(\underline{r}, t))$	dynamics of the fluorophore on the single-particle level:
$\delta\sigma$ :	fluctuations in the molecular absorption cross-section
$\delta q$ :	fluctuations in the quantum yield
$\delta C(\underline{r}, t)$ :	fluctuations in the local particle concentration at time $t$ , e.g. because of Brownian motion

Determining all these parameters is extremely difficult or even impossible. In order to simplify equation 3, the convolution factor of the two dimensionless spatial optical transfer functions  $I_{ex}(\underline{r})/I_0 * S(\underline{r})$  can be combined into a single function  $W(\underline{r})$ , which describes the spatial distribution of the emitted light. Often, this is approximated by a three-dimensional Gaussian, which is decayed to  $1/e^2$  at  $r_0$  in lateral direction and for  $z = z_0$  in axial direction:

$$W(\underline{r}) = e^{-\frac{2x^2+y^2}{r_0^2}} \cdot e^{-\frac{2z^2}{z_0^2}} \quad \text{Equation 4}$$

The remaining parameters  $\kappa, \sigma$  and  $q$  can be combined with the excitation intensity amplitude  $I_0$  to give a parameter that determines the photon count rate per detected molecule per second:  $\eta_0 = I_0 \cdot \kappa \cdot \sigma \cdot q$ . This parameter can be a measure for the signal-to-noise ratio of the measurement and therefore often used for a quick comparison regarding the quality of different adjustments or setups.

Using this information, equation 3 now reads

$$\delta F(t) = \int_V W(\underline{r}) \delta(\eta C(\underline{r}, t)) \cdot dV \quad \text{Equation 5}$$

The normalized autocorrelation function is defined as:

$$G(\tau) = \frac{\langle \delta F(t) \cdot \delta F(t + \tau) \rangle}{\langle F(t) \rangle^2} \quad \text{Equation 6}$$

The signal is analyzed with respect to its self-similarity after the lag time  $\tau$ . The autocorrelation amplitude  $G(0)$  is therefore merely the normalized variance of the fluctuating fluorescence signal  $\delta F(t)$ .

Substituting equation 5 into equation 6 yields:

$$G(\tau) = \frac{\iint W(\underline{r}) W(\underline{r}') \langle \delta(\eta \cdot C(\underline{r}, t)) \delta(\eta \cdot C(\underline{r}', t + \tau)) \rangle dV dV'}{\left( \int W(\underline{r}) \langle \delta(\eta \cdot C(\underline{r}, t)) \rangle dV \right)^2} \quad \text{Equation 7}$$

We can now separate the fluctuation term

$$\delta(\eta \cdot C(\underline{r}, t)) = C\delta\eta + \eta\delta C.$$

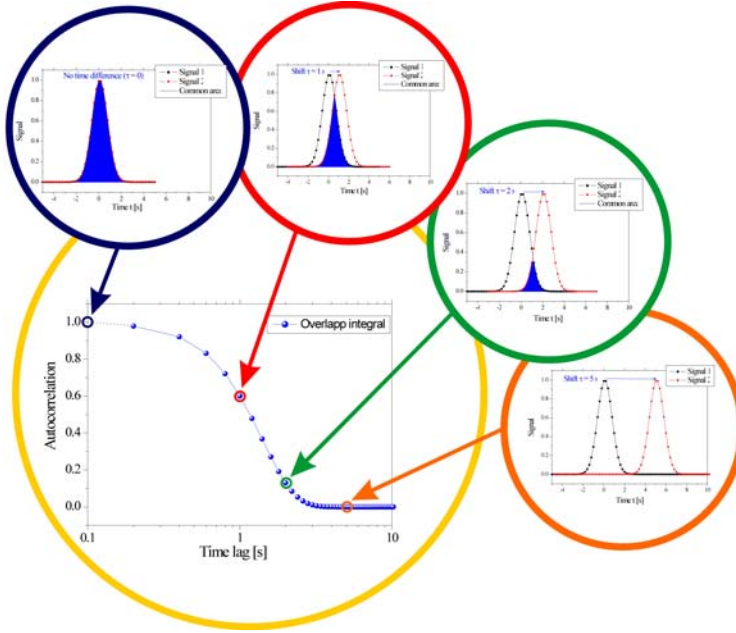


**Figure 8: Development of an autocorrelation curve.**

Obviously, equation 7 will be simplified to a large extent, if either the concentration or the parameter  $\eta$  are constant for a given system. Assuming first that the chromophore's fluorescence properties are not changing within the observation time, i.e.  $\delta\eta = 0$ , equation 7 can be rewritten as

$$G(\tau) = \frac{\int \int W(\underline{r})W(\underline{r}') \langle \delta C(\underline{r}, 0)\delta C(\underline{r}', \tau) \rangle dVdV'}{\langle C \rangle \int W(\underline{r})dV}$$

Considering only particles that are freely diffusing in three dimensions with the diffusion coefficient D, the so-called number density autocorrelation term  $\langle \delta C(\underline{r}, 0)\delta C(\underline{r}', \tau) \rangle$  can be calculated:

$$\langle \delta C(\underline{r}, 0)\delta C(\underline{r}', \tau) \rangle = \langle C \rangle \frac{1}{(4\pi D\tau)^{\frac{3}{2}}} \cdot e^{-\frac{(\underline{r}-\underline{r}')^2}{4D\tau}}$$

$$\begin{aligned}
 G(\tau) &= \frac{\iint W(\underline{r})W(\underline{r}')\langle C \rangle \frac{1}{(4\pi D\tau)^{\frac{3}{2}}} \cdot e^{-\frac{(\underline{r}-\underline{r}')^2}{4D\tau}} dVdV'}{\langle C \rangle \left( \int W(\underline{r})dV \right)^2} \\
 &= \frac{1}{\langle C \rangle (4\pi D\tau)^{\frac{3}{2}}} \frac{\iint W(\underline{r})W(\underline{r}') \cdot e^{-\frac{(\underline{r}-\underline{r}')^2}{4D\tau}} dVdV'}{\left( \int W(\underline{r})dV \right)^2}
 \end{aligned}$$

Inserting two more conventions, this finally leads to the expression for the normalized three-dimensional diffusion autocorrelation function for one species of molecules. First, you must consider the relationship between the lateral diffusion time  $\tau_D$  that a molecule stays in the focal volume, and the diffusion coefficient D, which is independent of the particular setup used:

$$\tau_D = \frac{r_0^2}{4 \cdot D} \quad \text{Equation 8}$$

Using this and the following definition of the effective focal volume  $V_{\text{eff}}$ ,

$$V_{\text{eff}} = \frac{\left( \int W(\underline{r})dV \right)^2}{\int W^2(\underline{r})dV} \stackrel{\text{equation 4}}{=} \frac{\left( \int e^{-2\frac{x^2+y^2}{r_0^2}} \cdot e^{-2\frac{z^2}{z_0^2}} dV \right)^2}{\int e^{-4\frac{x^2+y^2}{r_0^2}} \cdot e^{-4\frac{z^2}{z_0^2}} dV} \stackrel{\text{integration over space}}{=} \pi^{\frac{3}{2}} \cdot r_0^2 \cdot z_0 \quad \text{Equation 9}$$

one can finally calculate the autocorrelation function for one freely diffusing species of molecules:

$$G(\tau) = \frac{1}{V_{\text{eff}} \langle C \rangle} \cdot \frac{1}{\left(1 + \frac{\tau}{\tau_D}\right)} \cdot \frac{1}{\sqrt{1 + \left(\frac{r_0}{z_0}\right)^2 \cdot \frac{\tau}{\tau_D}}} \quad \text{Equation 10}$$

The first factor of equation 8 is exactly the inverse of the average particle number in the focal volume. Therefore, by knowing the dimensions  $r_0$  and  $z_0$  from calibration measurements, the local concentration of fluorescent molecules can be determined very exactly from the amplitude  $G(0)$  of the autocorrelation curve:

$$G(0) = \frac{1}{\langle N \rangle} = \frac{1}{V_{\text{eff}} \cdot \langle C \rangle} \quad \Leftrightarrow \quad \langle C \rangle = \frac{1}{V_{\text{eff}} \cdot G(0)} \quad \text{Equation 11}$$

The diffusion coefficient can be easily derived from the characteristic decay time of the correlation function  $\tau_D$  as mentioned above.

Hitherto, it was assumed that the chromophore's fluorescence properties are not changing while it is traversing the laser focus, i.e.  $\delta\eta = 0$ . Unfortunately, this assumption does not hold for real

dyes and higher excitation powers. The most common cause for such a “flickering” in the fluorescence intensity is the transition of the dye to the first excited triplet state. As this transition is forbidden by quantum mechanics, the chromophore needs a comparably long time to relax back to the ground state. During these intervals, the dye cannot emit any fluorescence photons and appears dark. Indeed, one can imagine the intersystem crossing as a series of dark intervals interrupting the otherwise continuous fluorescence emission of the molecule on its path through the illuminated region.

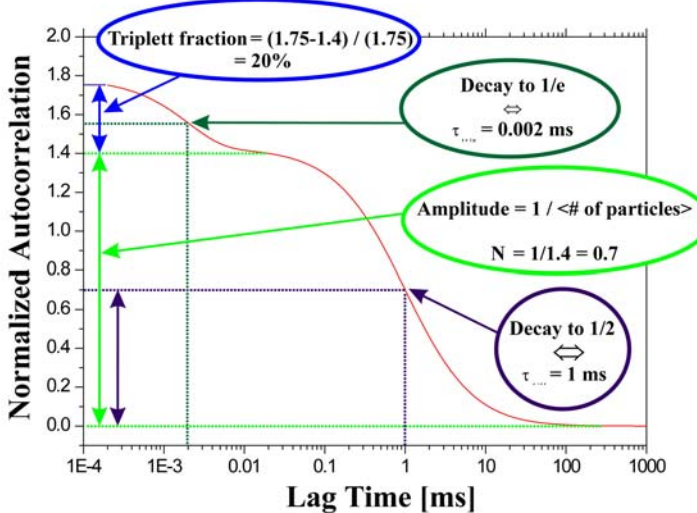


**Figure 9: Autocorrelation curve with fast triplet dynamics. The different parameters are explained in detail.**

Instead of recalculating the correct autocorrelation function for these slightly altered conditions, a much simpler and more general form that can be used. If intra- or intermolecular reactions give rise to fluorescence fluctuations on time-scales much faster than those caused by the mere movement of the particles, a separation of the dynamics is possible:

$$G_{\text{total}}(\tau) = G_{\text{motion}}(\tau) \cdot X_{\text{kinetics}}(\tau) \quad \text{Equation 12}$$

Of course, this assumption holds only for situations, in which the diffusion coefficient is unaltered by the reaction [Palmer 1987, Widengren 1998]. The triplet blinking mentioned above can be described by a simple exponential decay  $X_{\text{triplet}}(\tau)$

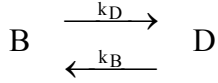
$$X_{\text{triplet}}(\tau) = 1 - T + T \cdot e^{-\frac{\tau}{\tau_{\text{triplet}}}}, \quad \text{Equation 13}$$

which shows as an additional shoulder in the measured curves for short time scales. It is also possible to normalize this expression by dividing by (1-T) [Widengren 1995, Schwille 2000]. Inserting equations 8 and 10 into eq. 9, the overall autocorrelation function for a freely diffusing dye can be written as:

$$G_{total}(\tau) = X_{kinetics}(\tau) \cdot G_{motion}(\tau)$$

$$= (1 - T + T \cdot e^{-\frac{\tau}{\tau_{triplett}}}) \cdot \frac{1}{V_{eff} \langle C \rangle} \cdot \frac{1}{(1 + \frac{\tau}{\tau_D})} \cdot \frac{1}{\sqrt{1 + \left(\frac{r_0}{z_z}\right)^2 \cdot \frac{\tau}{\tau_D}}}$$

The triplet blinking can be generalized to any fast photophysical phenomenon that results in reversible transitions between a bright - fluorescent – state B, and a dark state D in which no photons are emitted:



In analogy to equation 11, one can write:

$$X_{flickering}(\tau) = 1 - F + F \cdot e^{-\frac{\tau}{\tau_F}} \quad \text{Equation 14}$$

with  $\tau_F = \frac{1}{k_D + k_B}$  : relaxation time

$F = \frac{k_D}{k_D + k_B}$  : average fraction of dark molecules  
 $\hat{=} \text{ average fraction of time a molecule spends in the dark state}$

If the dark state D is not completely dark, the molecular emission yields  $\eta_i$  of the two states have to be taken into account to get the correct expression for F:

$$F = \frac{k_D k_B (\eta_B - \eta_D)^2}{(k_D + k_B)(k_B \eta_B^2 + k_D \eta_D^2)}$$

There may also be reactions, however, that do influence the mobility of the particle in some way. In this case, equation 9 must be generalized to take into account all different kinds of possible motion, weighted with the relative emission rate:

$$G_{motion}(\tau) = \frac{1}{V_{eff}} \frac{\sum_{\substack{\text{all different} \\ \text{species}}} \eta_i \langle C_i \rangle M_i(\tau)}{\left( \sum_i \eta_i \langle C_i \rangle \right)^2} \quad \text{Equation 15}$$

The motility-term  $M_i(\tau)$  must be adapted to the particular case. Besides the free three-dimensional diffusion discussed above, there are numerous other possibilities:

Free 3D diffusion:

$$M_i(\tau) = \frac{1}{\left(1 + \frac{\tau}{\tau_{d,i}}\right) \cdot \sqrt{1 + \left(\frac{r_0}{z_0}\right)^2 \cdot \frac{\tau}{\tau_{d,i}}}} \quad \text{Equation 16a}$$

Free 2D membrane diffusion

$$M_i(\tau) = \frac{1}{\left(1 + \frac{\tau}{\tau_{d,i}}\right)} \quad \text{Equation 16b}$$

Active transport with velocity  $v_i$

$$M_i(\tau) = e^{-\left(\frac{\tau v_i}{r_0}\right)^2} \quad \text{Equation 16c}$$

In natural membranes and inside living cells, the ideal case of Brownian diffusion does often not apply, because the movement of the particles is restricted or the mobility shows strong local changes [Schwille 1999, Wachsmuth 2000]. These deviations may be due to the confinement of the particles within cellular compartments or lipid domains in membranes, but also to nonspecific interaction of the diffusing molecules with other molecules or cellular structures. Regarding diffusion within membranes, the complex composition might also lead to an altered topology and thus to a changed mobility. Up to now, this phenomenon of anomalous diffusion is not completely understood. For various reasons, the mean square displacement is no longer directly proportional to time, but rather depends on  $t^\alpha$ , so that in above equations  $\tau/\tau_{d,i}$  has to be replaced by  $(\tau/\tau_{\text{anom},i})^\alpha$  [Feder 1996]:

$$\langle r^2 \rangle \propto t^\alpha \Leftrightarrow \frac{\tau}{\tau_{d,i}} \rightarrow \left( \frac{\tau}{\tau_{\text{anom},i}} \right)^\alpha \quad \text{with } \alpha < 1$$

No conventional diffusion constant can be defined in this case, and  $\tau_{\text{anom},i}^\alpha = r_0^2 / \Gamma_i$  with  $\Gamma_i$  being a transport coefficient of fractional time dimension.

Local confinement of the diffusion to organelles of a size comparable to that of the focal volume element requires even more sophisticated models. For example, trying to describe the particle motion within neuronal dendrites by the models mentioned above will fail completely. In such cases, complex non-analytic solutions of the correlation function have to be considered to appropriately model the biological situation [Gennerich 2000].

As depicted in figure 10, it is to some extent possible to distinguish the different molecular processes by the characteristic shape of the autocorrelation function. As a rule of thumb, the curves for anomalous subdiffusion decay more gradually than those for free diffusion, whereas active transport leads to a steeper, more abrupt decay. The latter may also apply for attractive or repulsive interactions between the particles under study.

Provided the time resolution of the setup is sufficient, an additional kinetic process may be determined: Rotational Brownian diffusion. To enhance the temporal resolution and overcome dead-times of the detector, the signal can be split onto two avalanche photodiodes and cross-correlated.

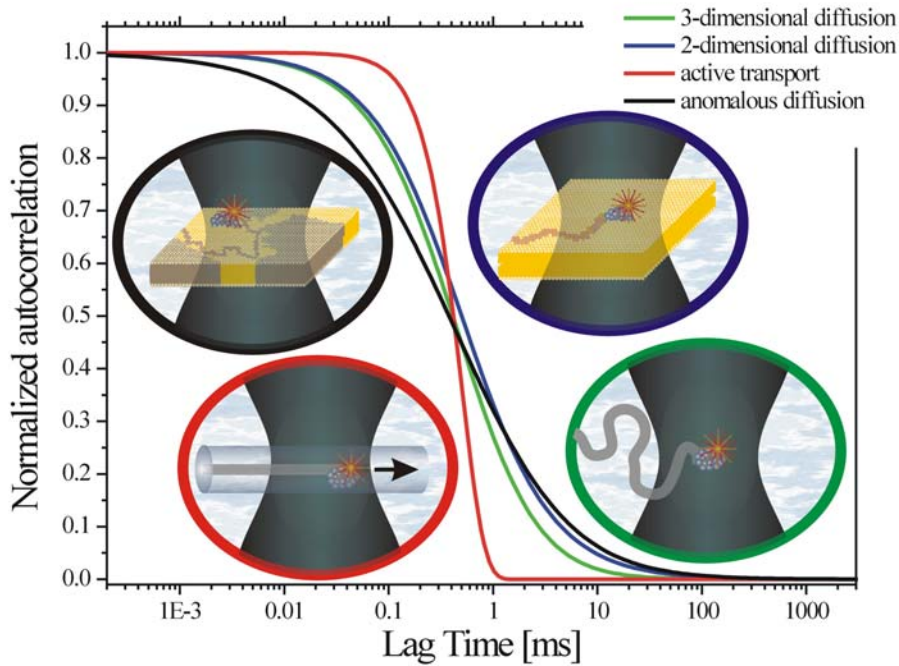


**Figure 10: Model autocorrelation curves for different kinds of particle motion**

As the chromophore absorbs light preferentially when it is polarized parallel to its absorption dipole, “correctly” oriented molecules will be more likely to be excited. This phenomenon is also known as *photoselection*. However, the photon emitted after the fluorescence lifetime  $\tau$  will be polarized in direction of the emission dipole of the dye molecule. If either the sample is excited with linearly polarized light at low intensity or detection is polarization-dependent (or both), rotation of the particles leads to observable fluctuations in the fluorescence signal [Kask 1987]. For GFP, the rotational correlation time in buffer solution is of the order of 20 ns, which agrees well with time-resolved anisotropy measurements [Widengren 1999]. Depending on the actual measurement conditions, i.e. the excitation, detection and the shape of the molecule, the theoretical description is quickly turning out to be extremely complicated [Ehrenberg 1974, Aragón 1975, Ehrenberg 1976].

For the slow rotational motion of a spherical diffusor, Aragón and Pecora [Aragón 1975] calculated the approximate solutions for different experimental geometries. If the rotational correlation time  $\rho$  is much larger than the fluorescence lifetime  $\tau_{\text{Fluorescence}}$ , the rotational correlation function thus can be written as

$$\begin{aligned} G_{\text{rot}}(\tau) &= A_{\text{rot}} \cdot (c_1 \cdot e^{-6\Theta\tau} + c_2 \cdot e^{-20\Theta\tau}) \\ &= A_{\text{rot}} \cdot \left( c_1 \cdot e^{\frac{\tau}{\rho}} + c_2 \cdot e^{\frac{-3\tau}{10\rho}} \right) \end{aligned} \quad \text{Equation 17}$$

[Eggeling 1999]. The relative amplitudes  $c_1$  and  $c_2$  are listed below:

<b>Excitation</b>	<b>Detection</b>	<b><math>C_1</math></b>	<b><math>C_2</math></b>
Linearly Polarized	Parallel	80	64/9
Linearly Polarized	Perpendicular	20/9	4
Linearly Polarized	All	860/9	4
Unpolarized	Parallel	5/9	16/9
Unpolarized	Perpendicular	215/9	1
Unpolarized	All	20	1

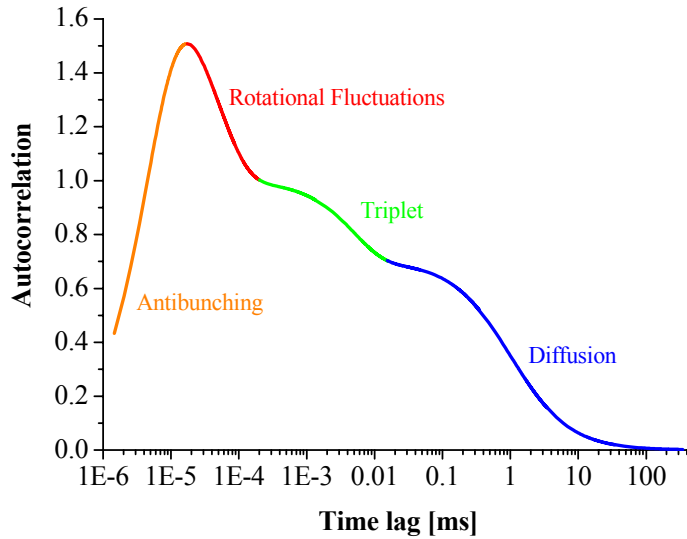


Figure 11: Timescales of various processes monitored by autocorrelation analysis

Considering experimental errors, e.g. polarization mixing due to high aperture objectives, the amplitudes may deviate from the theoretical values. Moreover, one exponential component can usually be neglected [Kask 1987, Widengren 1999] (For example, for polarized excitation and detection of the complete signal,  $c_1/c_2 = 860/(9 * 4) = 23.9$  )

The fastest process that can be monitored by FCS is the statistics of fluorescence emission itself. It merely describes the finite probability for a chromophore to emit a photon at time  $t$  given the last one was emitted at  $t = 0$ . This so-called *antibunching* shows up as an initial rise of the autocorrelation curve in the time range of the fluorescence lifetime.

$$G_{\text{antibunching}}(\tau) = -\frac{9}{5} \cdot e^{-\frac{\tau}{\tau_{\text{fluorescence}}}}$$

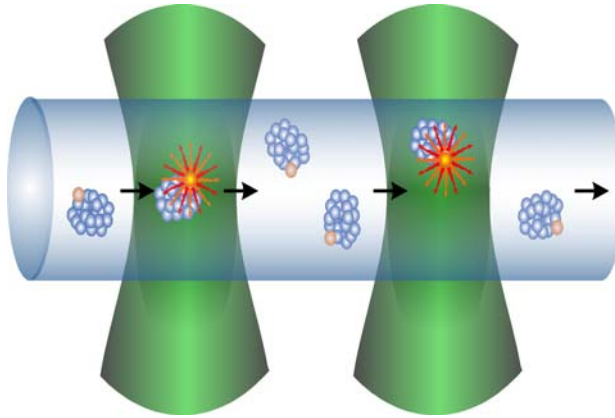
Equation 18

Figure 11 shows a schematic autocorrelation curve and the timescales of the different processes mentioned above. However, one needs to be careful interpreting the first few points given by any correlation, because here artifacts, e.g. detector noise, are most likely to be introduced.

### 3.2. Cross-correlation analysis

Performing an autocorrelation analysis, one effectively compares a measured signal with itself at some later time and looks for recurring patterns. In electronics it has been common practice for decades to correlate two different signals and thus e.g. get a measure for the crosstalk. In fact, cross-correlation analysis is just the straightforward way to generalize the method described above. Looking out for common features of two independently measured signals, one not only removes unwanted artifacts introduced by the detector (e.g. the so-called “afterpulsing” of an APD or intensity fluctuations of the illumination source), but also provides much higher detection specificity. Moreover, the quantities to be correlated need not be both fluorescence traces. Rather, they can be any physical quantity that can be measured – or even calculated – sufficiently fast to

reveal single particle fluctuations. Indeed, it is also possible to record only the arrival times of individual photons, as done by time-correlated single photon counting TCSPC, determine both the fluorescence intensity trace and interesting parameters after the actual measurement has been finished and perform a software-cross-correlation to reveal any dependencies.



**Figure 12: Dual-beam cross-correlation**

In spite of all these different possibilities to cross-correlate nearly any parameters, two applications have proved to be especially effective. First, there is the spatial cross-correlation between the fluctuations measured in two separate volume elements. As one molecule only correlates with itself, this kind of correlation curve will reach its maximum not for small time lags, but rather for the average time a molecule needs to travel from one detection volume to the other. Thus, the flow- or transport-velocity of the fluorescent particles can be determined [Brinkmeier1999].

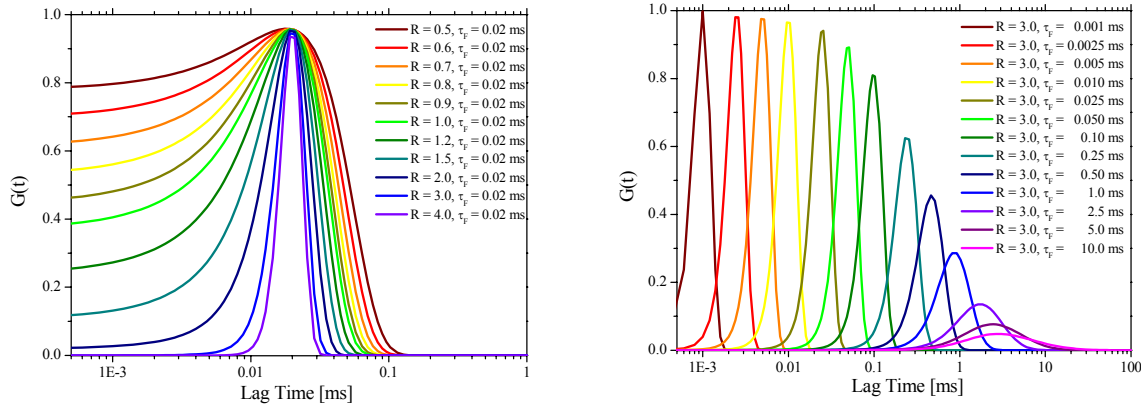


**Figure 13: Calculated spatial autocorrelation curves for two different experimental situations:**  
For the curves on the left-hand side, the ratio of focal diameter and distance of the two foci (and thus the overlap) was varied and the flow time kept constant, whereas on the right-hand side the effect of varying flow times can be studied.

In the case of directed flow in an arbitrary direction and three-dimensional diffusion, you get:

$$G(\tau) = \frac{1}{N} \cdot \frac{e^{-\frac{1}{\left(1+\frac{\tau}{\tau_{diff}}\right)} \left[ \left( \frac{\tau}{\tau_{flow}} \right)^2 + 1 - 2 \cdot \frac{\tau}{\tau_{flow}} \cos\left(\varphi \frac{\pi}{180^\circ}\right) \right]}}{\left(1 + \frac{\tau}{\tau_{diff}}\right) \cdot \sqrt{1 + \left(\frac{r_0}{z_0}\right)^2 \cdot \frac{\tau}{\tau_{diff}}}}$$

**Equation 19**

The flow velocity  $v$  is defined as  $v = \frac{\text{waist diameter of the focus}}{\text{flow time}} = \frac{r_o}{\tau_{flow}}$  and  $\varphi$  is the angle (in degrees) between the flow direction and the connecting line between the two foci.

The other prominent example of cross-correlation is the dual-color mode. As described briefly above, two spectrally different dyes are excited within the same detection element using two overlapping laser beams and separate detection pathways [Schwille 1997, Schwille 2001]. Dual-color cross-correlation is an extremely powerful tool to probe interactions between different molecular species, and a number of experiments have been carried out applying this technique to different kinds of reactions. There is only one principal prerequisite: the two differently labeled educts have to move independently at first and are then being fused together during the reaction, or vice versa.

The theoretical formalism can be briefly described in analogy to the autocorrelation theory. Generalizing equation 5, the fluctuating signals recorded in the two detection channels are given as

$$\begin{aligned}\delta F_1(t) &= \int W_1(\underline{r}) \eta_1 \delta(C_1(\underline{r}, t) + C_{12}(\underline{r}, t)) dV \\ \delta F_2(t) &= \int W_2(\underline{r}) \eta_2 \delta(C_2(\underline{r}, t) + C_{12}(\underline{r}, t)) dV\end{aligned}\quad \text{Equation 20}$$

with  $W_i(\underline{r})$  spatial intensity distribution of the fluorescence emission for species  $i$  ( $i = 1, 2$ )  
 $C_i(\underline{r}, t)$  concentrations for the single labeled species  $i$  ( $i = 1, 2$ )  
 $C_{12}(\underline{r}, t)$  concentration of the double-labeled species

The motion of the different components is supposed to be described by the term  $M_i(\tau)$  (cf. eq. 12). Assuming ideal conditions, where both channels have identical  $W_i(\underline{r})$  (and thus the same effective volume element  $V_{\text{eff}}$ ), fully separable emission spectra and a negligible emission-absorption overlap integral, the following correlation curves can be derived:

$$\begin{aligned}\text{Autocorrelation: } G_i(\tau) &= \frac{\langle \langle C_i \rangle M_i(\tau) + \langle C_{12} \rangle M_{12}(\tau) \rangle}{V_{\text{eff}} (\langle C_i \rangle + \langle C_{12} \rangle)^2} \quad \text{with } i = 1, 2 \\ \text{Crosscorrelation: } G_x(\tau) &= \frac{\langle C_{12} \rangle M_{12}(\tau)}{V_{\text{eff}} (\langle C_1 \rangle + \langle C_{12} \rangle)(\langle C_2 \rangle + \langle C_{12} \rangle)}\end{aligned}\quad \text{Equation 21}$$

[Schwille 2001].

There is, however, one additional advantage of this technique in comparison to the autocorrelation mode: If there is no reaction-induced quenching or fluorescence enhancement, and no particle exchange in the sample, the amplitude of the cross-correlation function is directly proportional to the concentration of double labeled particles. Knowing the amplitudes of the autocorrelation curves and thus, the concentrations of both single-labeled species, the concentration  $\langle C_{12} \rangle$  can be determined from equation 21 as follows:

$$\langle C_{12} \rangle = \frac{G_x(0)}{G_1(0) \cdot G_2(0) \cdot V_{\text{eff}}} \quad \text{Equation 22}$$

A correct evaluation of concentrations measured by cross-correlation requires good prior knowledge of the system or a careful calibration procedure of the two basic parameters resulting from FCS analysis, the effective volume element and the lateral characteristic residence time.

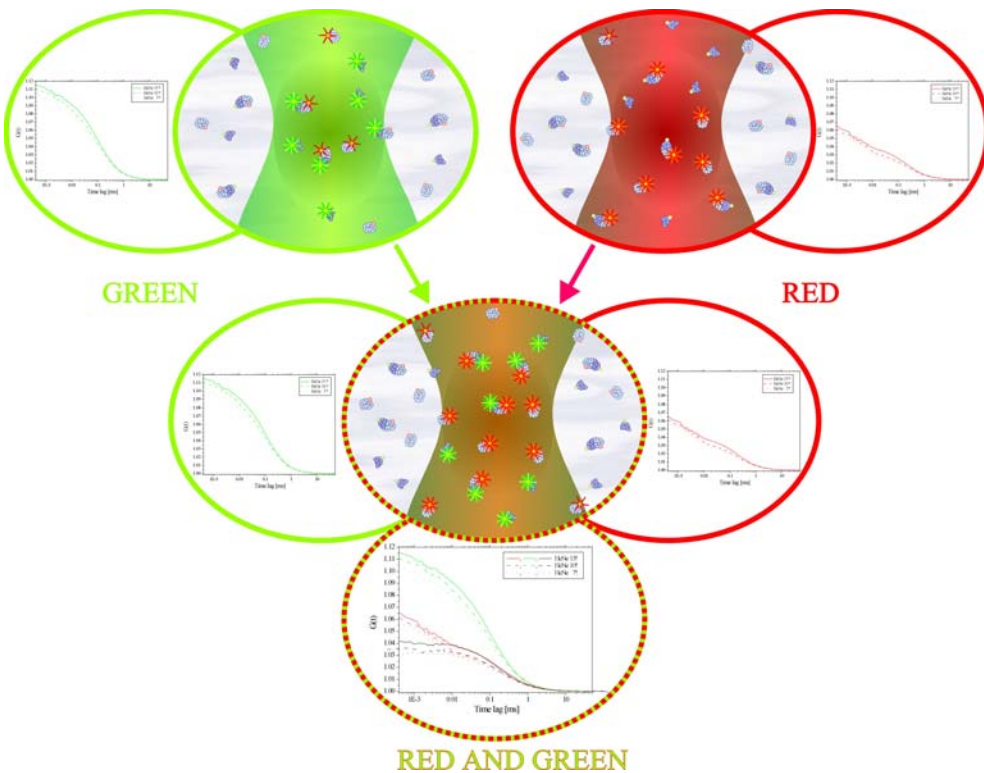


**Figure 14:** Using dual-color cross-correlation, more information about double-labeled particles can be received than from both single-color measurements.

## 4. FCS applications

### 4.1. Concentration and aggregation measurements

Now one might ask the question what actually can be learnt from the autocorrelation amplitudes about a particular system, provided one has succeeded in recording the curves. In order to find an answer, we must briefly return to the derivation of the autocorrelation formalism in chapter 3. It was already stated there that the autocorrelation amplitude  $G(0)$  is by definition the normalized variance of the fluctuating fluorescence signal  $\delta F(t)$ . Using this definition and combining it with Poissonian statistics that applies for ensembles of very few molecules, it became evident that  $G(0)$  equals the reciprocal number of molecules  $N$  in the effective volume element  $V_{\text{eff}}$  (equation 9). Thus in principle, absolute local concentrations can be determined very precisely if the size of the confocal volume element  $V_{\text{eff}}$  is known [Eigen 1994, Thompson 1991, Schwille 1997]. This, however, is not as easy as it may sound. Since FCS experiments are restricted to nanomolar concentrations, a variety of complications has to be dealt with. First, most protein molecules tend to adhere to any surfaces like cover slips or the walls of reaction chambers due to their surface

charges. For more concentrated solutions, this effect passes unnoticed. In the nanomolar and sub-nanomolar range, a significant amount of the molecules contained in the sample may simply disappear that way, unless specially coated containers are used. Second, photophysical damage may reduce the number of detected molecules even further, so that an overall accuracy for N of more than 20-30% is hard to achieve *in vitro*. There is an alternative approach for calibrating the excitation volume that does not rely on the exact knowledge of one concentration for comparison. If the diffusion coefficient D of one molecular species has been very precisely determined by some other technique, it is possible to calibrate  $r_0$  and  $z_0$  by using the fit parameters for  $\tau_D$  and  $r_0/z_0$  from the autocorrelation curve.

The determination of relative local concentrations is much more exact, because it does not depend on the size of the detection volume. When performing intracellular measurements, this can be useful to control expression levels of the intrinsically fluorescent proteins GFP or DsRed. Of course, it is also possible to load a cell with fluorescently labeled reagents, e.g. by electroporation, and control the increase in concentration by FCS.

Another parameter of crucial importance is the molecular brightness  $\eta$  that also has been mentioned before. This parameter is calculated by dividing the average fluorescence count-rate by the number of molecules within the illuminated region:

$$\eta = \frac{\langle F(t) \rangle}{N} = \langle F(t) \rangle \cdot G(0)$$

Although it is mainly used to quantify the performance of fluorescent probes or the quality of a particular setup, this brightness parameter is much more versatile: Knowing  $\eta$  it is also possible to rate fluorescence quenching due to a changed environment of the chromophore, or the fluorescence enhancement of single particles due to aggregation effects [Chen 2000].

Calculating not only the variance (i.e. the second moment), but also higher moments of the fluorescence signal can provide interesting additional information. Higher order autocorrelation analysis, as introduced by Palmer and Thompson [Palmer 1989], can be used to identify subpopulations differing only by their respective molecular brightness values. Whereas most chemical reactions affect the fluorescence quantum efficiency, only very few cause mobility changes large enough for a separation by standard autocorrelation analysis. In spite of its high susceptibility to noise, this kind of brightness distribution analysis has become the method of choice for many applications in biomolecular screening [Schaertl 2000, Klumpp 2001]. Only recently it is more and more substituted by photon counting histogram analysis, which is a static method complementary to FCS and can be done using the same setup.

## 4.2. Consideration of residence times: determining mobility and molecular interactions

### 4.2.1 Diffusion analysis

The determination of mobility-related parameters of biologically relevant molecules is one of the primary goals of FCS analysis in aqueous solution, and one it is especially suitable for. The sub-micrometer spatial resolution also makes it a useful technique for intracellular measurements. When trying to figure out how biological processes work in detail, it is essential to distinguish between diffusion or active transport, anomalous subdiffusion or even convection. Signal transduction or metabolic regulatory pathways can only be understood once the underlying transport mechanisms are revealed and well characterized. Because supporters of the FCS technique initially had to struggle with background suppression and unwanted photobleaching, the FRAP (fluorescence recovery after photobleaching) method has long been preferred for *in vivo* motility studies. The latter requires much higher dye concentrations and is thus less liable to suffer from the autofluorescence background (for detailed discussion of FCS versus FPR, see Ref. [Petersen 1986]). However, the temporal resolution is mainly limited to the millisecond time scale, so that FCS offers both higher dynamic performance and increased sensitivity. Low chromophore concentrations and laser power suffice for this equilibrium measurement, which is definitely less stressful for the cells under investigation.

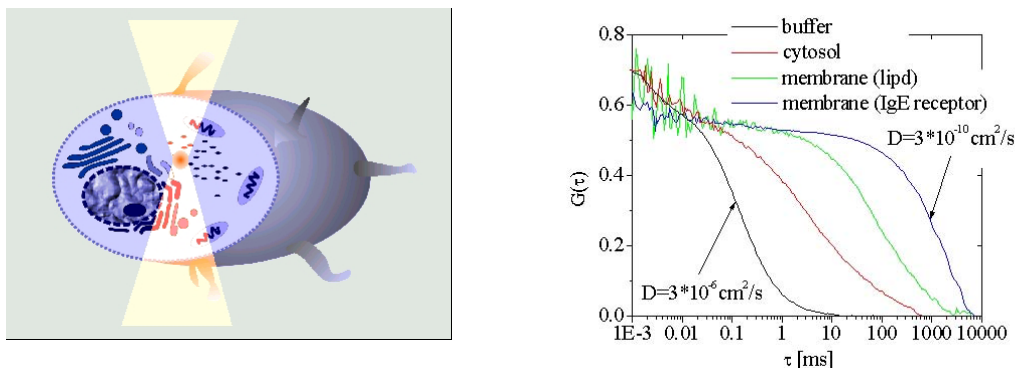


**Figure 15:** Various autocorrelation curves demonstrating the enormous difference in motility between buffer solution and cytosol

However, because of this inherent sensitivity, the proper selection of dyes is crucial. You always must be aware of the fact that the dyes might interfere with the monitored mechanism or introduce their own dynamics to the system. Many standard dyes, such as Rhodamines and Cyanines, are highly lipophilic and tend to associate to intracellular membranes, inducing severe deviations from free diffusion in the cytosol.

In figure 15, a selection of intracellular measurements is depicted. It is quite obvious that the mobility of the fluorophores strongly depends on the environment. The half-value decay time of the curves, which allows for a crude estimation of the mobility of the chromophore, varies by several orders of magnitude between the small dye in buffer and the large labeled receptor on the plasma membrane. The corresponding diffusion coefficients that can be calculated from the

decay times using equation 8 range from  $3 \times 10^{-6}$  cm<sup>2</sup>/s for the free dye to  $10^{-10}$  cm<sup>2</sup>/s for the bulky receptor.

### 4.2.2 Confined and anomalous diffusion

It is known from other techniques such as FRAP or particle tracking that membrane-bound receptors often exhibit anomalous subdiffusion. As outlined above, the mean square displacement of the molecules is in this case not proportional to the measurement time t, but exhibits a fractal time dependence [Bouchaud 1990, Saxton 1993]. Among possible reasons for such a non-Brownian behavior are environmental heterogeneities (e.g. different lipid phases or rafts), non-specific interactions with other particles or local confinement. About the underlying principles for non-homogeneous diffusion can only be speculated. It is quite astonishing that not only membrane-bound proteins exhibit such a strange motility, but also the lipids themselves show deviations from the normal homogeneous diffusion in natural cell membranes [Schwille 1999]. To exclude any label-induced artifacts, measurements in single-phase model membranes of giant unilamellar vesicles (GUVs) have been performed. In these idealized model systems, the lipids indeed show a perfectly homogeneous 2D diffusion. An altered membrane composition of the model membranes, resulting in a distinctive phase separation, however led to multiple diffusion coefficients for the labeled lipids [Korlach 1999]. Therefore one might assume that environmental heterogeneities play a key role in the anomalous subdiffusion phenomenon.

The term “anomalous subdiffusion” is not restricted to intracellular phenomena. Quite to the contrary, it is applied to any behavior that cannot be described by homogeneous diffusion and for which no other explanation holds. One alternative possibility is e.g. the gradual changes in the diffusion coefficient during protein folding or unfolding. Because of the complex nature of biological systems, it often requires evidence from various measurements to clearly rule out any artifacts before the motility can be termed truly anomalous. The cytosolic curve in figure 15 is an example for anomalous diffusion caused by the interactions of the dye with the cellular environment. The increased viscosity of the cytosol compared to the buffer solution would mainly result in a parallel shift of the autocorrelation curve towards longer times. Here, however, the form of the curve is changing strongly, so that interactions with intracellular membranes must be suspected [Schwille 1999a]. If the dye is replaced by the rather inert GFP, normal diffusion in the cytoplasm can be observed [Dittrich 2000]. The diffusion coefficient is 3-4 times reduced relative to buffer measurements, which corresponds to the increased viscosity. As has been shown recently, the diffusion of EGFP in the nucleus suddenly becomes anomalous as well, although it is perfectly homogeneous in the cytosol [Wachsmuth 2000]. This may justify the assumption that the topology of cellular organelles has a non-negligible effect on the diffusional properties.

### 4.2.3 Active transport phenomena in tubular structures

When looking on a molecular scale, even such an apparently simple organism like a single cell is a highly complicated system. The many different substances needed for the cell’s metabolism

have to be exactly at the right place at the right time for the cell to sustain its biological function. There are various possibilities for a molecule to be transferred from the place it is produced to where it is needed. Obviously, the simplest means of transportation is diffusion along a concentration gradient. No complicated mechanism is required for this rather unspecific way. However, such a substance must be rather ubiquitous within the cell, as the majority of the molecules are serving only to maintain the concentration gradient. Thus, it is generally much more effective for the cell to use directed transport along an internal tubular network, resembling the coverage of a country with motorways. Much work is presently devoted to characterize the endocytic and secretory trafficking pathways of proteins or vesicles, or receptor internalization in signal transduction. FCS is well suited for distinguishing between diffusive and oriented motions of dilute molecules on a sub-millisecond time-scale. For very slow processes on time-scales of several seconds to minutes, time-lapse imaging has been successfully employed. Fascinating images could be recorded showing GFP-labeled proteins being transported through the various compartments of the secretory pathway [Hirschberg 1998]. Recently, a commercial instrument (ConfoCor II, Zeiss, Jena) has combined fluorescence microscopy, confocal laser scanning microscopy and FCS in one setup. This demonstrates both the mutual dependence of the techniques and the complementary information to be gained.

Already in 1978, the theoretical background was laid for analyzing different active transport processes such as laminar flow or a combination of directed plug flow and diffusion [Magde 1978]. For the latter, the diffusion autocorrelation function must be expanded by an exponential term. Assuming a transport velocity  $v_f$  so that a molecule needs the time  $\tau_f = x_0/v_f$  to cross the focal volume, the function reads:

$$G(\tau) = \frac{1}{N} \cdot \frac{1}{1 + \frac{\tau}{\tau_D}} \cdot \frac{1}{\sqrt{1 + \left(\frac{t_0}{x_0}\right)^2 \frac{\tau}{\tau_D}}} \cdot e^{-\left(\frac{\tau}{\tau_f}\right)^2 \frac{1}{1 + \frac{\tau}{\tau_D}}} \quad \text{Equation 23}$$

Whereas there are examples describing FCS analysis of a laminar flow obeying Hagen-Poiseuille's law, or the uniform electroosmotic flow, measurements of active transport phenomena in living cells are still scarce.

As an example, the mobility of GFP targeted to the plastid stroma in tubular structures interconnecting separate plastids in vascular plants was investigated using FCS [Köhler 2000]. As exchange of GFP between different interconnected plastids was obviously possible, the major task of FCS analysis consisted in revealing the nature of the extremely slow transport phenomenon. For this study, 2-photon excitation was chosen because of the higher background suppression and increased toleration by plant cells. Positioning the laser focus directly on a microtubule, it could be shown that most of the GFP was contained within vesicular structures. Thus, it is indeed actively transported, although in rather large batches, and superimposed to anomalous diffusion.

#### 4.2.4 Determination of molecular interactions

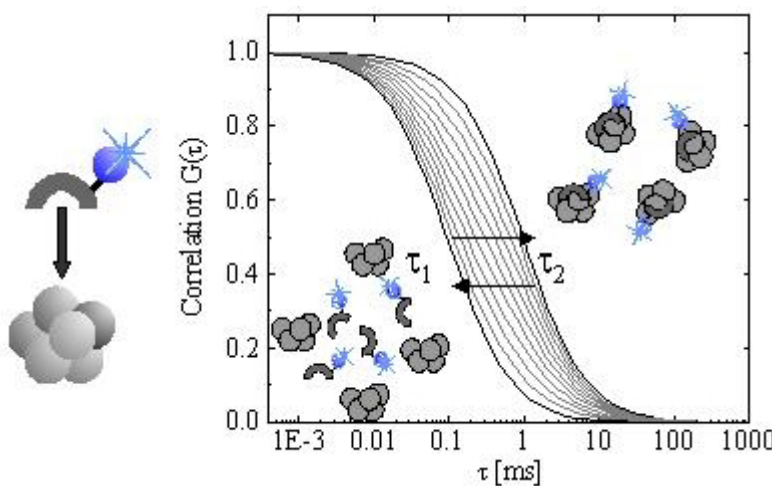


**Figure 16: Changes in diffusion time of a small ligand upon binding to a heavy protein**

parameters like e.g. the diffusion time, molecular brightness or concentration can be determined. An ideal reaction system consists of one small, labeled ligand and a comparatively large, non-fluorescent counterpart. For a significant change in the diffusion time, the mass ratio should be at least eight, preferably more than an order of magnitude, due to the approximate cube root dependence of the diffusion coefficient on molecular mass (see below). Analyzing the system is especially easy, if only one fluorescent species (e.g. fully free or fully bound ligand) is present at the start and the end of the association process. During the reaction, the percentage of the complex will continuously increase, until chemical equilibrium is reached or one species has completely reacted. Therefore, it is possible to determine the diffusion time of the labeled ligand from a reference measurement. Then, the other curves can be fitted with two diffusing components, fixing the diffusion time of the smaller component to the value determined beforehand [Schwille 1997]. Kinjo and Rigler [Kinjo 1995] first established this principle to follow the binding kinetics of short fluorescent DNA probes to a longer DNA target; the same measurement scheme was further applied to a comparison of hybridization kinetics of DNA probes with different binding sites to folded RNA [Schwille 1996]. Mobility analysis has meanwhile proven to be an extremely powerful tool for a large variety of ligand-receptor systems [Schüler 1999, Wohland 1999, Margeat 2001].

Another situation where the mobility of molecules can be altered dramatically is when membrane binding is involved. When a molecule adheres to the membrane itself or to membrane proteins such as receptors, both the diffusion type (two-dimensional instead of three-dimensional) and the characteristical time scale are changed. Recently, first applications in cell cultures were reported, investigating the binding and displacement of proinsulin C-peptide [Rigler 1999], and EGF [Pramanik 2001] to and from cell membranes.

In the previous sections, the usefulness of FCS for determining mobility coefficients with high spatial resolution was emphasized. The majority of FCS applications, however, hitherto has been concerned with reactions occurring on a much larger time scale than the short time window given by the residence time of a molecule within the measurement volume. Such reactions can be easily followed by continuous FCS monitoring, i.e. successive autocorrelation curves are recorded with shortest integration time possible. From those curves, changes in the accessible

#### 4.2.5 Conformational changes

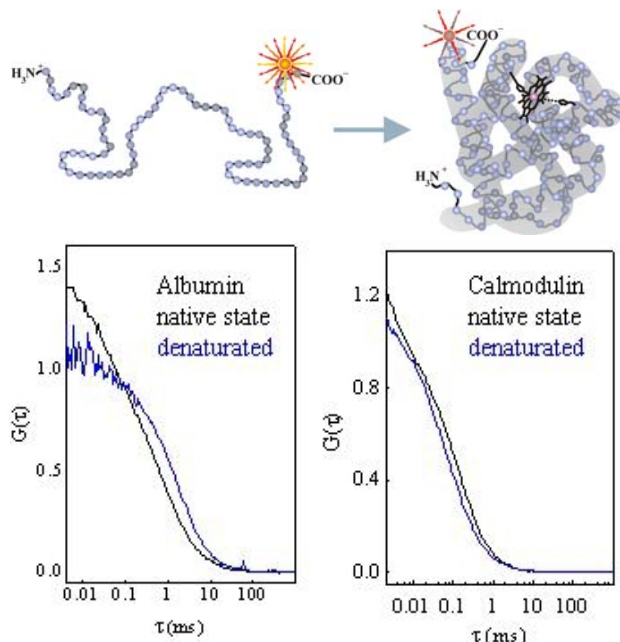


**Figure 17:**  $R_h$  is usually smaller for globular molecules than for elongated ones and can thus be used to determine the folding state of proteins. **Bottom:** examples for changes in diffusion coefficients following protein denaturation. Albumin in the denatured state exhibits longer diffusion times  $\tau_d$ , while denatured Calmodulin tends to diffuse faster with shorter  $\tau_d$

Dependent on the tertiary structure of proteins, denaturation does not necessarily increase the hydrodynamic radius. In cases where the native structure comprises stiff lobes such as in calmodulin, denaturation can actually lead to a more globular shape with smaller hydrodynamic radius.

Recapitulating the various aspects of mobility analysis discussed above, it is evident that FCS is a versatile tool for these applications, provided the changes in diffusion coefficient are large enough. Assuming that a change in the diffusion coefficient of a factor two would be sufficient, and approximating the particle by a homogeneous sphere, the hydrodynamic radius will scale with the third root of the molecular weight. Therefore, a globular protein would need to gain about eight times its own mass, which is often not the case in interesting biochemical reactions. In spite of its attractiveness, this approach is thus only applicable to a limited number of possible reaction systems.

Changes in the diffusion coefficient of a particle can not only be induced by chemical reactions, but by any other phenomenon causing changes in the hydrodynamic radius  $R_h$ . The diffusion coefficient in an aqueous solution of viscosity  $\eta_v$  is given by the Stokes-Einstein relationship

$$D = \frac{k \cdot T}{6\pi \cdot \eta_v \cdot R_h} \quad \text{Equation 24}$$

Therefore any changes in the hydrodynamic radius will directly affect the mobility of the molecule. A more massive particle will usually have a larger volume and thus an increased  $R_h$ . However, also the three-dimensional structure and thus, the shape, of a protein influence its mobility, such that it is in principle possible to monitor protein folding or unfolding transitions. The differences in the diffusion coefficients between two folding states are generally quite small, this is why only few measurements on this topic have been published yet [Borsch 1998].

### 4.3. Consideration of cross-correlation amplitudes: a direct way to monitor association/dissociation and enzyme kinetics

The obvious solution to this dilemma is dual-color cross-correlation. Although the required setup is considerably more expensive, due to the second laser and detector, and also more difficult to adjust, this technique is much more versatile, and data analysis can be significantly simplified [Kettling 1998]. In contrast to the autocorrelation applications described above that focus mostly on analysis of the functional form of the correlation curves, the most important parameter is now simply the cross-correlation amplitude. As outlined in the theory section, this amplitude is a direct measure for the concentration of double-labeled particles diffusing through the focal volume. In principle, one simply focuses on the occurrence of coincident fluctuations in the two emission channels, induced by concerted motion of spectrally distinguishable labels. All kinds of reactions leading either to a separation or an association of the two labeled species can thus be

monitored. Under ideal conditions (i.e. no crosstalk between the detectors), the amplitude  $G_x(0)$  is zero unless double-labeled particles are present in the sample. This makes fast yes-or-no decisions based on this parameter feasible.

The tremendously enhanced detection specificity was first shown on association reactions of two small complementary DNA oligonucleotides carrying green and red labels, respectively [Schwille 1997]. It was proven that the absolute concentration of the dimer could be directly monitored by crosscorrelation.

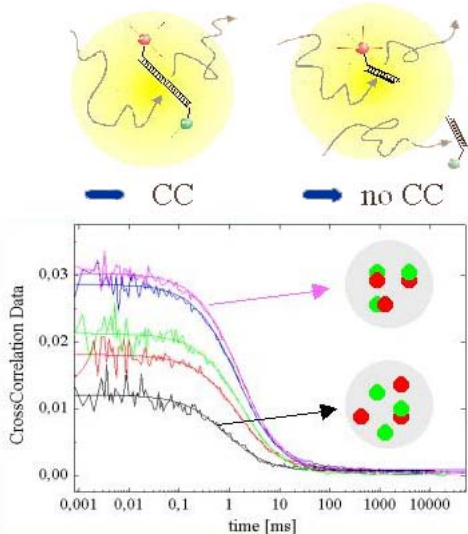


**Figure 18: Cross-correlation measurement**

On basis of dual-color cross-correlation, Kettling et al. [Kettling 1998] demonstrated a biologically very attractive approach to characterize enzyme kinetics at extremely low enzyme concentrations ( $> 1.6 \text{ pM}$ ). The assay to be tested was the cleavage of double-labeled dsDNA by *EcoRI* restriction endonuclease.

The inherently simple information provided by this

technique, where yes/no decisions about enzyme activity could be made just by recording the cross-correlation amplitude, renders it very attractive for fast screening applications. The acquisition time per sample could be reduced to less than a second, without substantially impairing the reliability [Koltermann 1998].

#### 4.3.1 Two-photon cross-correlation analysis

Denk et al. [Denk 1990, Denk 1995] first demonstrated that two-photon excitation is an elegant solution to obtain intrinsic 3D resolution in laser scanning microscopy, with the additional advantage that photodamage of dye resources and cellular compounds in studies on live samples can be confined to the immediate vicinity of the focal plane. This allows specific illumination of interesting sites in the living cell and eliminates photodamage effects in off-focus areas. By applying two-photon excitation to intracellular FCS (Schwille 1999a), it could indeed be verified that in comparison to conventional one-photon FCS, two-photon excitation at the same signal

levels minimizes photobleaching in spatially restrictive cellular compartments, thereby preserving long-term signal acquisition. The expected advantages known from imaging applications, such as reduced scattering and higher penetration depths in turbid tissue could also be verified. However, there is one more essential feature in respect to one-photon excitation: the two-photon induced transition to the excited state, which is formally symmetry forbidden, exhibits different selection rules and vibronic coupling. As a consequence, the two-photon excitation spectra of many common fluorophores differ considerably from their one-photon counterparts without any change in emission, which makes it possible to accomplish simultaneous excitation of spectrally distinct dyes.

Although the concept of multicolor excitation has previously been utilized in confocal imaging applications (Xu 1997), its suitability for single molecule based techniques, requiring the detection of two labels on a single molecule within the limited time frame of a molecule's dwelling in the focal spot, has so far not been demonstrated. Clearly, the choice of a proper dye system is crucial for such applications, because the chosen dyes should not only exhibit similar excitation and distinct emission spectra, but also comparable photobleaching quantum yields at a given wavelength and intensity.

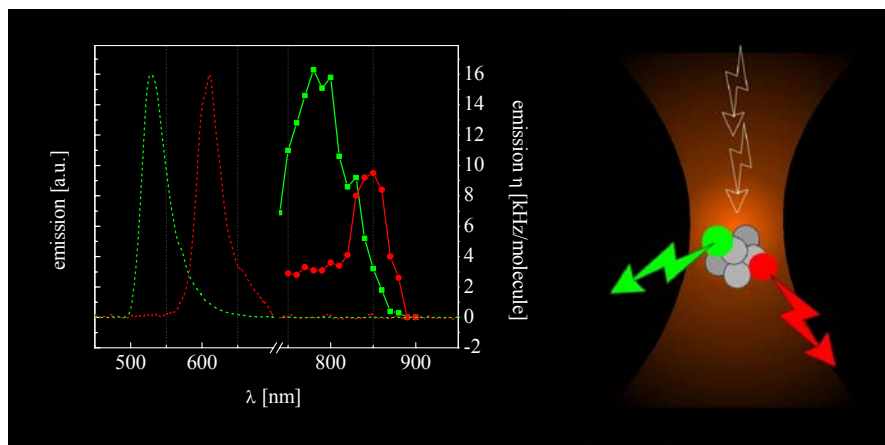


**Figure 19:**  
Simultaneous two-photon cross-correlation spectroscopy (TPCCS): The idea is to excite two spectrally distinct dyes (e.g. Rhodamine Green and Texas Red) with a single IR laser line. The emission spectra are not affected by the two-photon process. The two-photon excitation spectra show a clear overlap.

Dual-color two-photon excitation with a single laser line has recently been accomplished in the Schwille laboratory (Heinze 2000) in a cross-correlation scheme, simultaneously accessing two fluorescent species with minimal spectral overlap in their emission properties, Rhodamine Green and Texas Red (Fig. 19). The experimental setup is significantly simplified compared to confocal cross-correlation FCS geometries, because only one laser line is used for excitation and no pinholes are in principle required in the detection pathway. The critical task in two-photon dual-color cross-correlation is to find a system of suitable dyes that not only exhibit minimal spectral overlap in their emission characteristics, but also tolerate the same excitation intensities without considerable photobleaching. Thus, an optimization procedure of both parameters, wavelength and intensity, has to be performed to find a compromise of optical conditions for which the dyes exhibit similar performance. For that purpose, the excitation wavelength is scanned with the tunable laser between 740 nm and 900 nm, and the fluorescence emission yield  $\eta$ , measured in photon count rate per single detected molecule, is recorded for both dyes independently. Figure 19 shows a plot of  $\eta$  for both Rhodamine green and Texas Red versus the two-photon excitation wavelength. During the scan, laser intensity and pulse-width are controlled and kept constant at

30 mW and 100 fs. The optimal wavelength for the following cross-correlation experiments where both dyes are excited equally well, appeared to be 830 nm.

The concept was experimentally demonstrated with the established *EcoRI* endonuclease assay introduced above for one-photon FCCS (Heinze 2000), using the mentioned dye pair. Meanwhile, a large variety of other possible dye combinations for dual and even triple color excitation could be identified.

#### **4.4. Consideration of fast flickering: intramolecular dynamics and probing of the microenvironment**

As a last example, the effect of fast fluctuations in the fluorescence emission on the autocorrelation curve shall be analyzed. Among the mechanisms leading to fast reversible changes in the fluorescence emission yield are intramolecular reversible quenching due to electron transfer [Widengren 1997, Edman 1996], light-induced blinking due to a protonation reaction in several GFP mutants [Schwille 2000] and photoisomerization as observed for Cyanine dyes. Also, dynamic FRET (fluorescence resonance energy transfer) on a single molecule level may be considered, although the underlying mechanism is different.

As already indicated above, there is a much more common phenomenon leading to blinking on fast time-scales: At the high excitation rates applied for FCS measurements, the quantum mechanically forbidden transition between the first excited singlet and triplet state becomes increasingly probable. This so-called intersystem crossing in fact occurs in most dyes, due to their complex photophysical nature. The excited state lifetime for the triplet state is usually several orders of magnitude larger than the fluorescence lifetime. It can be up to several microseconds. Mathematically, the corresponding fast dynamics part of the autocorrelation function can be described by equation 13. The triplet state parameters depend mainly on the excitation intensity, but also the environment of the dye may have some influence. Molecular oxygen is one of the most common triplet state quenchers, but also some heavy metal ions have been shown to alter the triplet state kinetics [Widengren 1998]. This sensitivity to ion concentrations could potentially be useful for probing the intracellular environment.

But not only the ion concentration can be determined, there is also a number of chromophores that exhibit pH-dependent emission characteristics, being useful tools probe the local pH. The most commonly known single-molecule pH-meter is GFP, the cloneable green fluorescent protein, being particularly suited for intracellular applications. Predominantly the long-wavelength mutants EGFP (enhanced GFP) and YFP (yellow fluorescent protein) show an interesting emission behavior on time-scales between micro- and milliseconds, which is easily accessible to FCS [Schwille 2000]. Haupts et al. [Haupts 1998] identified a reversible protonation of the chromophore of EGFP to be responsible for the flickering dynamics. In bulk solution of EGFP, the average fluorescence emission is known to decrease to zero at low pH ( $pK_a = 5.8$ ) paralleled by a decrease of the absorption at 488 nm and an increase at 400 nm.

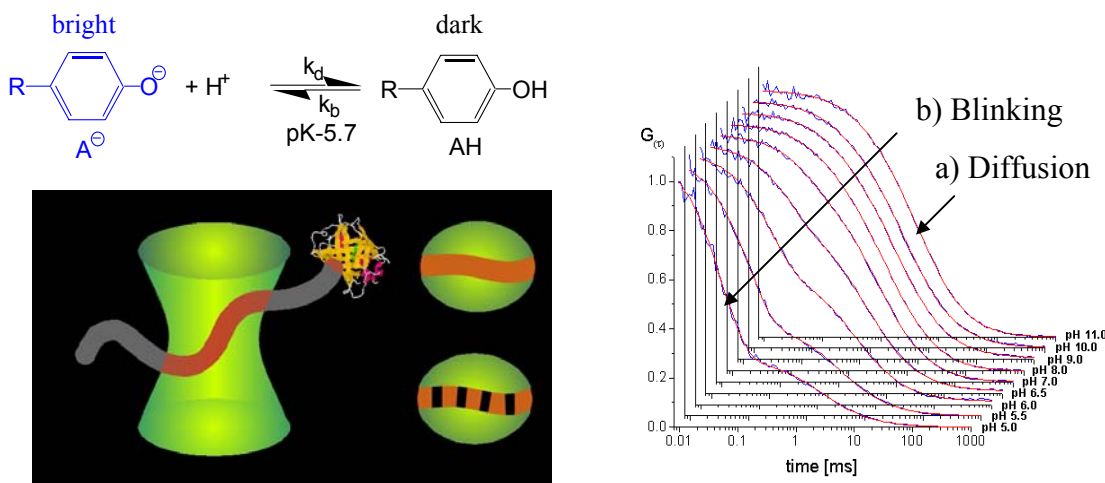


**Figure 20:** This is the reaction scheme showing the transition from bright (deprotonated) to dark (protonated) state of the dye for excitation at 488 nm. On the right hand side you can see the autocorrelation curves measured in buffer solutions of different pH.

In a single-molecule measurement, time resolved measurements of the fluorescence emission are possible and promptly offer a solution to this problem. Upon protonation of the chromophore, a spectral shift in the absorption spectrum is caused. Therefore, it is no longer possible to excite the molecule with the selected laser line and it appears dark. As for the triplet blinking, the autocorrelation function shows an additional fast kinetic component, which can be described by the same mathematical formalism. The time constant of the protonation induced flickering decreases with pH as expected, while the average fraction of molecules in the non-fluorescent (i.e., protonated) state increases to over 80% at pH 4.5. As this effect only depends on the pH of the surrounding medium, it can readily be employed as an intrinsically calibrated and very sensitive probe.

## 5. Conclusions and outlook

Fluorescence correlation spectroscopy has been proven to be a very versatile technique for both *in vivo* and *in vivo* applications. Based on light irradiation only, it is minimally invasive and thus extremely useful for investigating biological systems. As this method is concerned with fluctuations around the thermodynamic equilibrium, no external stress has to be applied to determine the relaxation parameters. The confocal setup guarantees high spatial resolution, which is combined with its inherently high temporal resolution to render it complementary to most other fluorescence techniques. A large number of parameters can be determined by FCS, among them not only the mobility constants and concentrations, but also fast internal dynamics and photophysical processes. The accessible time-scales range from several sub-microseconds to several hundred milliseconds. The observation of very slow processes is limited by the finite photochemical lifetime of fluorophores, if they are exposed to strong illumination intensities.

## 6. References

- Aragón, S. R.; Pecora, R.; *Biopolymers* **14**, 119 (1975)
- Bouchaud, J.P.; Georges, A.; *Phys. Rep.* **195**, 127 (1990)
- Brinkmeier,M.; Dörre, K.; Stephan, J.; Eigen, M.; *Anal. Chem.* **71**, 609 (1999)
- Chen, Y.; Müller, J.D.; Tetin, S.Y.; Tyner, J.D.; Gratton, E.; *Biophys. J.* **79**, 1074 (2000)
- Denk,W.; Strickler,J.H.; Webb,W.W.; *Science* **248** (4951), 73 (1990)
- Denk,W.; Piston,D.W.; Webb,W.W. in *Handbook of Biological Confocal Microscopy*, Pawley,J.B. Eds., Plenum Press, New York, (1995) p. 445ff
- Dittrich, P.; Malvezzi-Campeggi, F.; Jahnz, M.; Schwille, P.; *Biol. Chem.* **382**, 491 (2000)
- Edman, L.; Mets, Ü.; Rigler, R.; *Proc. Natl. Acad. Sci. USA* **93**, 6710 (1996)
- Eggeling, C.; Fries, J.R.; Brand, L.; Guenther, R.; Seidel, C.A.M.; *Proc. Natl. Acad. Sci. USA* **95**, 1556 (1998)
- Ehrenberg, M.; Rigler, R.; *Chem. Phys.* **4**, 390 (1974)
- Ehrenberg, M.; Rigler, R.; *Quart. Rev. Biophys.* **9**, 69(1) (1976)
- Eigen, M. and Rigler, R., *Proc Natl. Acad. Sci. USA* **91**, 5740 (1994)
- Elson, E.L. and Magde, D., *Biopolymers* **13**, 1 (1974)
- Feder, T.J.; Brust-Mascher, I.; Slattery, J.P.; Baird, B.; Webb, W.W.; *Biophys. J.* **70**, 2767 (1996)
- Gennerich, A.; Schild, D.; *Biophys. J.* **79**, 3294 (2000)
- Haupts, U.; Maiti, S.; Schwille, P.; Webb, W.W.; *Proc. Natl. Acad. Sci. USA* **95**, 13573 (1998)
- Heinze, K.G.; Koltermann, A.; Schwille, P.; *Proc. Natl. Acad. Sci. USA* **97**, 10377 (2000)
- Hirschberg, K.; Miller, C.M.; Ellenberg, J.; Presley, J.F.; Siggia, E.D.; Phair, R.D.; Lippincott-Schwartz, J.; *J. Cell Biol.* **143**, 1485 (1998)
- Kask, P.; Piksamav, P.; Mets, Ü.; Pooga, M.; Lippma, E.; *Eur. Biophys. J.* **14**, 257 (1987)
- Kettling, U., Koltermann, A.; Schwille, P.; Eigen, M.; *Proc. Natl. Acad. Sci. USA* **95**, 14116 (1998)
- Kinjo, M.; Rigler, R.; *Nucleic Acids Res.* **23**, 1795 (1995)
- Klumpp, M.; Scheel, A.; Lopez-Calle, E.; Busch, M.; Murray, K.J.; Pope, A.J.; *J. Biomolec. Screening* **6**, 159 (2001)
- Köhler, R.H.; Schwille, P.; Webb, W.W.; Hanson, M.; *J. Cell Sci.* **113**, 3921 (2000)
- Koltermann, A.; Kettling, U.; Bieschke, J.; Winkler, T.; Eigen, M.; *Proc. Natl. Acad. Sci. USA* **95**, 1421 (1998)
- Korlach, J.; Schwille, P.; Webb, W.W.; Feigenson, G.F.; *Proc. Natl. Acad. Sci. USA* **96**, 8461 (1999)
- Magde, D., Elson, E.L.; Webb, W.W., *Biopolymers* **13**, 29 (1974)

- Magde, D., Elson, E.L.; Webb, W.W., *Biopolymers* **17**, 361 (1978)
- Margeat, E.; Poujol, N.; Boulahtouf, A.; Chen, Y.; Müller, J.D.; Gratton, E.; Cavailles, V.; Royer, C.A.; *J. Mol. Biol.* **306**, 433 (2001)
- Palmer, A.G.; Thompson, N.L.; *Biophys. J.* **51**, 339 (1987)
- Palmer, A.G.; Thompson, N.L.; *Proc. Natl. Acad. Sci. USA* **86**, 6148 (1989)
- Petersen, N.O.; Elson, E.L.; *Meth. Enzymol.* **130**, 454 (1986)
- Pramanik, A.; Rigler, R.; *Biol. Chem.* **382**, 371 (2001)
- Rigler, R.; Pramanik, A.; Jonasson, P.; Kratz, G.; Jansson, O.T.; Nygren, P.A.; Stahl, S.; Ekberg, K.; Johansson, B.L.; Uhlen, S.; Uhlen, M.; Jornvall, H.; Wahren, J.; *Proc. Natl. Acad. Sci. USA* **96**, 13318 (1999)
- Saxton, M.J.; *Biophys. J.* **64**, 1766 (1993)
- Schaertl, S.; Meyer-Almes, F.J.; Lopez-Calle, E.; Siemers, A.; Kramer, J.; *J. Biomolec. Screening* **5**, 227 (2000)
- Schüler, J.; Frank, J.; Trier, U.; Schäfer-Korting, M.; Saenger, W.A.; *Biochemistry* **38**, 8402 (1999)
- Schwille, P.; Oehlenschläger, F.; Walter, N.; *Biochemistry* **35**, 10182 (1996)
- Schwille, P.; Bieschke, J.; Oehlenschläger, F.; *Biophys. Chem.* **66**, 211 (1997)
- Schwille, P.; Meyer-Almes, F.-J.; Rigler, R.; *Biophys. J.* **72**, 1878 (1997)
- Schwille, P.; Korlach, J.; Webb, W.W.; *Cytometry* **36**, 176 (1999)
- Schwille, P.; Haups, U.; Maiti, S.; Webb, W.W.; *Biophys. J.* **77**, 2251 (1999a)
- Schwille, P.; Kummer, S.; Heikal, A.A.; Moerner, W.E.; Webb, W.W.; *Proc. Natl. Acad. Sci. USA* **97**, 151 (2000)
- Schwille, P.; in *Fluorescence correlation spectroscopy. Theory and applications*, Elson, E.L.; Rigler, R. Eds., Springer, Berlin, (2001) p. 360
- Thompson, N.L.; in *Topics in Fluorescence Spectroscopy*, Lakowicz, J.R. ; Ed., Plenum Press, New York (1991) Vol.1, p. 337
- Wachsmuth, M.; Waldeck, W.; Langowski, J.; *J. Mol. Biol.* **298**, 677 (2000)
- Widengren, J.; Mets, Ü.; Rigler, R.; *J. Chem. Phys.* **99**, 13368 (1995)
- Widengren, J.; Dapprich, J.; Rigler, R.; *Chem. Phys.* **216**, 417 (1997)
- Widengren, J.; Rigler, R.; *Cell. Mol. Biol.* **44**, 857 (1998)
- Widengren, J.; Mets, Ü.; Rigler, R.; *Chem. Phys.* **250**, 171 (1999)
- Winkler, T.; Kettling, U.; Koltermann, A.; Eigen, M.; *Proc. Natl. Acad. Sci. USA* **96**, 1375 (1999)
- Wohland, T.; Friedrich, K.; Hovius, R.; Vogel, H.; *Biochemistry* **38**, 8671 (1999)
- Xu, C. and Webb, W.W. in *Topics in Fluorescence Spectroscopy*, J. Lakowicz Ed., Plenum Press, New York (1997) Vol. 5, p.471